


Stress-Induced Acceleration and Ordering in Solid-State Dewetting

Francesco Boccardo^{1,*}, Fabrizio Rovaris², Ashwani Tripathi³, Francesco Montalenti², and Olivier Pierre-Louis^{1,†}

¹*Institut Lumière Matière, UMR5306 Université Lyon 1 - CNRS, 69622 Villeurbanne, France*

²*L-NESS and Department of Materials Science, University of Milano-Bicocca, Via R. Cozzi 55, I-20125 Milano, Italy*

³*Center for Soft and Living Matter, Institute of Basic Sciences, 44919 Ulsan, Republic of Korea*

 (Received 9 December 2020; revised 9 November 2021; accepted 19 December 2021; published 12 January 2022)

We report on the influence of elastic strain on solid-state dewetting. Using continuum modeling, we first study the consequences of elastic stress on the pinching of the film away from the triple line during dewetting. We find that elastic stress in the solid film decreases both the time and the distance at which the film pinches in such a way that the dewetting front is accelerated. In addition, the spatial organization of islands emerging from the dewetting process is affected by strain. As an example, we demonstrate that ordered arrays of quantum dots can be achieved from solid-state dewetting of a square island in the presence of elastic stress.

DOI: [10.1103/PhysRevLett.128.026101](https://doi.org/10.1103/PhysRevLett.128.026101)

Dewetting most often refers to the familiar process by which a liquid film on a solid substrate breaks up into droplets. In this process, mass is transported by hydrodynamic flows in the film, and the dynamics is driven by a gain in surface and interface energies [1–4]. Following the upsurge of nanosciences in the 1990s, observations of dewetting of solid films with nanoscale thickness have now become commonplace [5–8], both in semiconductors [9–18] and metal films [19–26]. Furthermore, strategies for the control of the size and spatial order of nanoislands emerging from solid-state dewetting have attracted much attention, driven by applications in nanotechnologies [7,18,27]. In solid-state dewetting, mass is usually transported by surface diffusion. This mechanism, which is efficient only at the nanoscale and for high enough temperatures, triggers specific dynamical features. One of the most striking consequences of surface diffusion is periodic film pinching behind the dewetting rim [20,28]. In this Letter, we show how spatiotemporal scales and ordering of islands formed by dewetting are influenced by a fundamental difference between solids and liquids, i.e., elasticity.

The role of elasticity on the nanoscale patterning of thin solid films has been a major issue, especially since the discovery of the Stranski-Krastanov growth mode, by which nanoislands (also called quantum dots) form spontaneously during deposition [29–32]. The destabilization of flat films leading to quantum dots originates from the Asaro-Tiller-Grinfeld (ATG) instability [33,34], in which part of the elastic energy caused by the lattice mismatch between the film and the substrate is released by surface corrugations.

We find that the dewetting of stressed solid films leads to an interplay between surface-diffusion instabilities (such as the pinching process) and the stress-induced ATG instability. We combine well-established continuum models,

including surface diffusion and elastic strain [35–38], with a wetting potential that accounts for a finite contact angle [39,40]. We show that periodic pinching is accelerated by elasticity. The timescale and length scale of pinching obey a scaling *Ansatz* involving the contact angle and a normalized elastic strength. These results are quantitatively compared with the decrease of the island size observed in experiments in stressed Si(100) films on amorphous SiO₂ substrates (sSOI) [17,41], which have been previously [7,42] discussed only on the basis of an energy balance discarding kinetics. Comparison with experimental data suggests a broad well of the wetting potential at the interface between Si and SiO₂. Beyond its influence on spatiotemporal scales, elastic strain also changes drastically the ordering of the islands emerging from the dewetting process. Indeed, the usually complex spatial organization of islands in unstressed square films [18,27] changes to ordered arrays of dots when the film is stressed.

Model.—Our model is based on the standard Mullins approach [43] for surface diffusion. We assume that all physical properties of the film and the substrate are isotropic. Mass conservation imposes that the normal velocity v_n of the interface obeys a continuity equation $v_n = -\nabla_s \cdot \mathbf{j}$, where ∇_s is the surface gradient. The surface flux \mathbf{j} is assumed to be proportional to the gradient of the local chemical potential $\mathbf{j} = -M\nabla_s\mu$, where the mobility M is taken to be constant for the sake of simplicity. This leads to an evolution equation for the height $h(x, y, t)$ of the free surface [43,44] (see the Supplemental Material [45]):

$$\partial_t h = \nabla \cdot (M\psi \cos \theta \nabla \mu), \quad (1)$$

where $\cos \theta = [1 + (\nabla h)^2]^{-1/2}$, i.e., θ is the angle of the local surface slope, ∇ is the gradient in the x, y plane, and ψ is a tensor with components $\psi_{xx} = 1 + (\partial_y h)^2$, $\psi_{yy} = 1 + (\partial_x h)^2$ and $\psi_{xy} = \psi_{yx} = -\partial_x h \partial_y h$.

The chemical potential $\mu = \mu_\gamma + \mu_w + \mu_{el}$ accounts for three contributions. The first one is the effect of surface tension [43] $\mu_\gamma = \Omega\gamma\kappa$, where γ is the surface tension, Ω is the atomic volume, and κ is surface curvature. The second contribution accounts for wetting effects and is a generalization of the disjoining pressure [37,39,40,55–59]

$$\mu_w = \Omega(w(h)\kappa + w'(h) \cos \theta), \quad (2)$$

where $w(h)$ is the film wetting potential. Partial wetting with a contact angle θ_{eq} is obtained with $w(h) = (1 - \cos \theta_{eq})\gamma W(h/h_w)$. The function $W(z)$ vanishes for large thicknesses $W(z \rightarrow \infty) = 0$, exhibits a single minimum $W(0) = -1$ at $z = 0$ that corresponds to the substrate height, and increases quickly for negative z . In equilibrium, this leads to the Young-Dupre relation [39] $\gamma \cos \theta_{eq} = w(0) - w(h)$. The potential width h_w is defined for any potential as the width of an equivalent square-well potential with the same depth [i.e., $\int_0^\infty dh w(h) = h_w w(0)$]. We have used three different types of potentials: (i) finite range $W(z > 7/2) = 0$, (ii) exponential [$W(z \gg 1) \sim -\exp(-3z/2)$], and (iii) van der Waals power law ($W(z \gg 1) \sim -z^{-2}$). The full expressions of $W(z)$ are reported in the Supplemental Material [45]. The numerical results reported in the main text are all obtained with the finite-range potential. In nonequilibrium conditions like those encountered during solid-state dewetting, the contact angle is close to its equilibrium value (for constant M), as discussed in details in Ref. [39].

In a seminal work, Wong *et al.* [28] have shown that solid-state dewetting dynamics induces pinching at a finite distance from the triple line, as shown in Fig. 1 (this is similar to the periodic formation of toroidal voids during the surface diffusion–induced merging of solid spheres [60]). For a flat film of initial thickness h_f , the distance λ_0 and time τ_0 between two consecutive pinching events were predicted for unstressed films with small θ_{eq} [28]:

$$\lambda_0 = \frac{h_f L_0}{\theta_{eq}}, \quad \tau_0 = \frac{h_f^4 T_0}{M \Omega \gamma \theta_{eq}^4}, \quad (3)$$

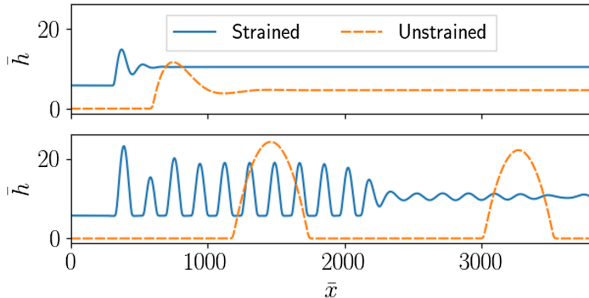


FIG. 1. Stress-induced acceleration of periodic mass shedding. One-dimensional simulations of strained ($\rho = 0.043$) and unstrained thin film, with $\bar{h}_f = 4.7$, $\theta_{eq} = 10^\circ$, and finite-range wetting potential. Time from top to bottom: strained, $\bar{t} = 2.3 \times 10^6$, 2.5×10^7 ; unstrained 2.3×10^7 , 4.4×10^8 .

where L_0 and T_0 are dimensionless numbers. Wong *et al.* found that $L_0 = L_0^* \approx 67.5$ and $T_0 = T_0^* \approx 217 \times 10^3$. These results correspond to the limit of a film thickness h_f much larger than the width of the wetting potential $h_f/h_w \rightarrow \infty$ [40]. When h_f/h_w is finite, mass shedding is accelerated by the attractive tail of the wetting potential [40]. We have checked that the dependence of λ_0 and τ_0 on θ_{eq} is still given by Eq. (3) for finite h_f/h_w (see the Supplemental Material [45]). However, L_0 and T_0 depend on h_f/h_w , as discussed in Ref. [40]. They tend to L_0^* and T_0^* when $h_f/h_w \rightarrow \infty$ and decrease with decreasing h_f/h_w in a way that depends on the details of the wetting potential profile (see Ref. [40] and the Supplemental Material [45]).

To our knowledge, there is no direct measurement of $w(h)$ in solid films. However, indirect information can be extracted from dewetting experiments. For example, mass shedding of thick Ni/MgO films with $h_f = 120$ nm indicated $\lambda_0 \approx 5 \mu\text{m}$ and $\tau_0 \approx 1255$ min [61]. As discussed in Ref. [40], using physical parameters from the literature [62–66], Eq. (3) with $L_0 = L_0^*$ and $T_0 = T_0^*$ predicts $\lambda_0 \approx 5 \mu\text{m}$ and $\tau_0 \approx 3604$ min in agreement with experiments. Hence, we conclude that, for Ni/MgO, $h_w \ll h_f = 120$ nm.

In the presence of elastic stress, a third contribution appears in the chemical potential [35,36,38,67,68]:

$$\mu_{el} = \frac{\Omega}{2} \sigma_{ij} u_{ij}, \quad (4)$$

where σ and u are, respectively, the stress and strain tensors. In the bulk, mechanical equilibrium imposes $\nabla \cdot \sigma = 0$ in the film and the solid. We assume identical elastic properties in the film and substrate for simplicity. At the free surface of the film, we have $\sigma \cdot \mathbf{n} = 0$, where \mathbf{n} is the surface normal. The interface between the film and the substrate is assumed to be flat with a normal vector in the z direction. We assume molecular adhesion with no slip at this interface to account either for lattice matching between a film and a substrate with different lattice parameters or for a strained crystalline film sticking on an amorphous substrate such as in sSOI. The interface imposes a strain $\eta = (a_s - a_f)/a_s$ in the film, where a_f is the unstressed bulk lattice parameter of the film material and a_s is the lattice parameter imposed by the contact to the substrate. The displacement relative to the reference state composed of a film with strain η and a substrate with no strain are assumed to be continuous across the film-substrate interface. In addition, we impose that $\sigma \cdot \mathbf{z}$ is continuous across the interface.

The linearization of the chemical potential for small perturbations of a flat film leads to [33,34]

$$\mu_{el} = -\Omega A_{el} \eta^2 \mathcal{H}(h), \quad (5)$$

where $A_{el} = 2(1 + \nu)E/(1 - \nu)$ depends on the Young's modulus E and the Poisson's ratio ν . Denoting the Fourier

transform with the variable \mathbf{q} of a function f as $\hat{f}_{\mathbf{q}}$, the operator \mathcal{H} is defined via its Fourier transform $\hat{\mathcal{H}}_{\mathbf{q}}(h) = |\mathbf{q}|\hat{h}_{\mathbf{q}}$. The integrodifferential operator \mathcal{H} is the Hilbert transform of the gradient of h as derived in Ref. [69] showing explicitly the long-range character of elastic interactions. The minus sign in Eq. (5) accounts for the decrease of the elastic energy when the film surface is corrugated. Hence, surface perturbations are unstable—this is the ATG instability. The wavelength and timescale emerging from this instability result from a balance between elastic relaxation and surface tension:

$$\lambda_{\infty} = \frac{8\pi}{3} \frac{\gamma}{A_{\text{el}}\eta^2}, \quad \tau_{\infty} = \frac{2^8}{3^3} \frac{\gamma^3}{\Omega M A_{\text{el}}^4 \eta^8}. \quad (6)$$

In the case of sSOI with $\eta = 0.8\%$ to $\eta = 1.6\%$ [41], we find $\lambda_{\infty} \approx 0.3$ to $0.07 \mu\text{m}$. (for better accuracy, we considered different elastic properties for the film and the substrate; see the Supplemental Material [45] and Refs. [37,57]). Since similar orders of magnitudes $\lambda_0 \approx 0.4 \mu\text{m}$ are obtained for the mass shedding wavelength from Eq. (3) for a $h_f = 7$ to 8 nm Si film as in sSOI experiments [41], we expect a nontrivial coupling between mass shedding and the ATG instability.

To investigate the full dynamics numerically, we define normalized variables $\bar{h} = h/h_w$, $\bar{x} = x/h_w$, $\bar{y} = y/h_w$, and $\bar{t} = t\Omega M \gamma/h_w^4$. Remark that since h and x are rescaled by the same factor, the angles θ are preserved. The normalized evolution equation for \bar{h} , reported in the Supplemental Material, depends on 3 dimensionless parameters: θ_{eq} , which accounts for wetting effects; $\rho = A_{\text{el}}\eta^2 h_w/\gamma$, which describes the balance between elasticity and surface tension; and Poisson's ratio ν . In the following, we use $\nu = 0.3$ so that the dynamics only depends on θ_{eq} and ρ .

Pinching simulations.—Simulations were performed via the coupling to a finite element elastic solver for the bulk elastic fields following an approach analogous to that of Ref. [32] (see the Supplemental Material [45] for more information) and using the finite-range wetting potential. A simulation starting with a film with a straight edge along the y direction is shown in Fig. 2. The pinching instability is still present when ρ is nonvanishing, leading to the formation of lines that subsequently break down into islands. Interestingly, no transversal fingering instability

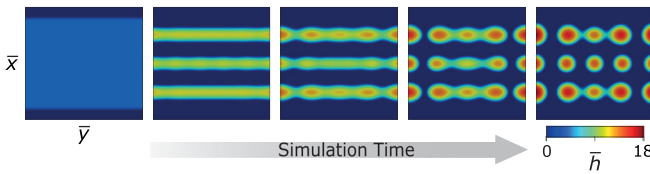


FIG. 2. Mass shedding in the presence of strain. Starting from a stripe, with $\bar{h}_f = 4.7$, $\theta_{\text{eq}} = \pi/4$, $\rho = 0.017$ and finite-range potential. The final simulation time is 1.46×10^7 .

is observed. A similar absence of fingering was reported recently for very thin films in the absence of elastic effects in Ref. [40]. Note also that fingering can be observed for some orientations and not for others in experiments [13,41] and in kinetic Monte Carlo simulations with anisotropy [70–72].

Since no transversal perturbation of the front along y is observed in Fig. 2 during the initial pinching process that forms lines, we resort to faster one-dimensional simulations, assuming translational invariance along y to analyze the pinching process. In addition, we use a linearized approximation of the elastic chemical potential [Eq. (5)], leading to $\bar{\mu}_{\text{el}}[\bar{h}; \nu] = \mathcal{H}(\bar{h})$ (a check of the quantitative agreement with the full solution is reported in the Supplemental Material [45]). An example of simulation is reported in Fig. 1. The normalized pinching distance $\bar{\lambda}$ and pinching time $\bar{\tau}$ both decrease with increasing ρ . The shape of the resulting islands is close to that of the isolated equilibrium islands as derived in Refs. [73,74]. Furthermore, the values of $\bar{\lambda}$ and $\bar{\tau}$ approach the predictions of the ATG instability [Eq. (6)] for large ρ , which read $\bar{\lambda}_{\infty} = 8\pi/(3\rho)$ and $\bar{\tau}_{\infty} = 2^8/(3^3\rho^4)$ in normalized coordinates.

Since $\bar{\lambda}$ is found to be independent of θ_{eq} for large ρ , and recalling that L_0 is also independent of θ_{eq} , we propose a simple scaling *Ansatz* $\bar{\lambda} = \theta_{\text{eq}}^{-1} g(\rho/\theta_{\text{eq}})$ with $g(u \rightarrow 0) = h_f L_0/h_w$ and $g(u \gg 1) = 8\pi/(3u)$. Similarly, we obtain $\bar{\tau} = \theta_{\text{eq}}^{-4} f(\rho/\theta_{\text{eq}})$ with $f(u \rightarrow 0) \rightarrow h_f^4 T_0/h_w^4$ and $f(u \gg 1) \rightarrow 2^8/(3^3 u^4)$. These scaling *Ansätze* are confirmed by data collapse in Figs. 3(a),(b).

Island density.—Experimental measurements of the increase of the final island density c_{exp} for increasing strain have been reported in Ref. [41] for sSOI islands results from the Rayleigh-Plateau-like instability [75,76] of the linear structures formed during the dewetting process. However, due to the absence of real-time *in situ* measurement for sSOI, it is not clear if such linear structures result from a pinching instability or from a fingering instability of the dewetting front, as suggested in Refs. [71,77,78]. Motivated by the observation that the distance between islands within a line in Fig. 2 is similar to the distance between the lines, we proceed with the simple assumption that the island concentration obeys $c_{\text{exp}} \approx c = 1/\lambda^2$.

Using our scaling *Ansatz*, we expect a reduction of the island density $c/c_0 = [g(0)/g(\rho/\theta_{\text{eq}})]^2$, so that $c/c_0 \rightarrow 1$ when $\rho \rightarrow 0$, and $c/c_0 \rightarrow [3\rho h_f L_0/(8\pi h_w \theta_{\text{eq}})]^2$ for large ρ . Considering L_0 as a fitting parameter, we see in Fig. 3(c) that $L_0 = 0.4L_0^*$ provides quantitative agreement with experiments. Anisotropy could affect the quantitative interpretation of this result because anisotropy can affect the profile of the rim and change the value of L_0 [79]. However, the pinch-off distance of metal films is quantitatively predicted by the isotropic prediction [Eq. (3)] with $L = L_0^*$ [40], and in addition previous modeling based on

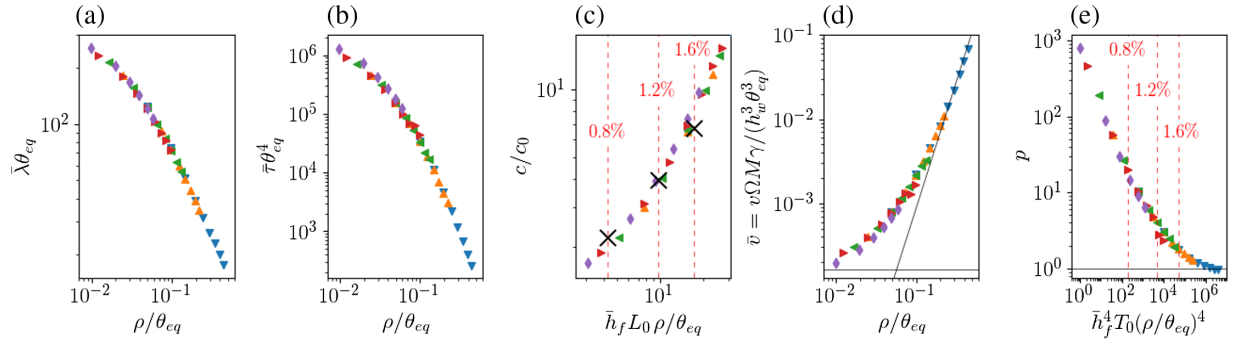


FIG. 3. Length scale and timescale of periodic mass shedding as a function of strain. Simulation results: (blue down pointing triangle) $\theta_{\text{eq}} = 10^\circ$, (orange up pointing triangle) $\theta_{\text{eq}} = 20^\circ$, (green right pointing triangle) $\theta_{\text{eq}} = 30^\circ$, (red left pointing triangle) $\theta_{\text{eq}} = 40^\circ$, (violet diamond) $\theta_{\text{eq}} = 50^\circ$. (a) Collapse of pinching wavelengths. (b) Collapse of pinching times. (c) Ratio c/c_0 of the island density under strain over the density at zero strain. Experimental results from Ref. [41]: (cross mark). (d) Velocity v at which the dewetting front invades the film by means of periodic pinching. (e) Number of pinching events p that can be observed before the destabilization of the film by the ATG instability.

an isotropic phase field model [18] has succeeded in reaching a quantitative description of the dewetting process of SOI films. Therefore, we use the value of L_0 calculated from our isotropic model.

We have studied the decrease of L_0 when increasing h_f/h_w for the finite-range, van der Waals, and exponential potentials (see the Supplemental Material [45]). We find that $L_0 = 0.4L_0^*$ corresponds to an effective potential width h_w between 1.7 and 3 nm. This value of h_w is much larger than the length scales suggested by usual microscopic descriptions of molecular interactions in Si-SiO₂ systems [80] and by first-principles calculations of wetting potentials (e.g., ~ 0.15 nm for Ge films on Si(001) [81,82]). Since the Si/SiO₂ interface is atomically flat [83–87], we do not expect any artificial increase of h_w due to interface roughness [88,89]. The high value of h_w could be related to the formation of a quasicrystalline SiO₂ layer (up to 3 nm), which is strongly dependent on the Si film thickness h_f , as suggested by Ref. [86]. Hence, the analysis of dewetting dynamics appears as a novel way to probe the physics of the wetting potential in solid films, following similar analyses for liquids [90]. In addition, since we find that h_f/h_w is not large (between 2 and 4), a finite potential width is necessary in order to capture the wetting effects in the dewetting dynamics of ultrathin SOI films.

The velocity at which the dewetting front invades the film via periodic pinching is $v = \lambda/\tau$. As seen in Fig. 3(d), v is accelerated by elastic effects and converges to the ATG velocity $\lambda_\infty/\tau_\infty$ for large elastic strain. However, the propagation of the dewetting front is limited by the emergence of the ATG instability in the film away from the dewetting front. The number of pinching events that can be observed before the destabilization of the film by the ATG instability far from the dewetting front is $p = \tau_\infty/\tau$ (up to fluctuation-induced corrections as discussed in Ref. [40] for initial roughness and Refs. [70,91,92] for

thermal noise). From the scaling Ansatz, we obtain $p = 2^8 \theta_{\text{eq}}^4 / [3^3 \rho^4 f(\rho/\theta_{\text{eq}})]$. Using $L_0 = 0.4L_0^*$ as obtained above, we find $p \approx 20, 5$, and 2 for $\eta = 0.8\%$, 1.2% , and 1.6% . These results suggest that, while the dewetting process is dominated by the propagation of the fronts for $\eta = 0.8\%$, it should be dominated by the ATG instability away from fronts for $\eta = 1.6\%$.

Lateral ordering.—Elastic strain also has a drastic effect on lateral ordering. To focus on spatial organization, we compare dewetting simulations of square films of width ℓ with various values of ρ , keeping a fixed ratio $n = \ell/\lambda = \bar{\ell}/\bar{\lambda}$. Simulations with $n = 4$ are shown in Fig. 4. While complex patterns can be obtained in the absence of elasticity [18,27], the ordering of the islands increases drastically in the presence of elastic stress, leading to an array of ordered quantum dots. Similar square films with $n = 3$ to 5 and their time evolution are presented in the Supplemental Material [45]. These results open novel perspectives in the design of complex patterns from films with various initial shapes in experiments [18,61] and simulations [18,93].

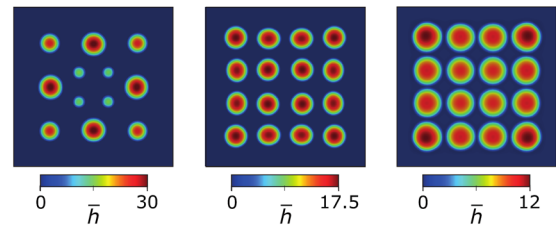


FIG. 4. Strain-induced ordering. Initial square film with a lateral size $\bar{\ell} = 4\bar{\lambda}$, height $h_f = 4.7$. Finite-range potential with $\theta_{\text{eq}} = \pi/4$. From left to right, $\rho = 0, 0.017$ and 0.037 , and $\bar{t} = 3 \times 10^8, 1.1 \times 10^7$, and 9×10^6 .

Conclusions.—In summary, elastic stress accelerates solid-state dewetting and produces smaller islands in agreement with experimental observations. Comparison with experiments reveals that the width of the wetting potential in SOI systems could be around 2 to 3 nm.

Acceleration of dewetting due to tensile residual stresses [94,95] that are linear in the stress and not accompanied with pinching was also found in slippery viscoelastic polymer films. In contrast, the acceleration of surface diffusion-limited dewetting of stressed solid films is quadratic in the stress (tensile and compressive stresses have similar consequences) and is intimately related to pinching. Hence, dewetting of complex fluids and plastic solids could exhibit novel behaviors that mix these two limits.

In addition, elastic stress changes drastically the order of solid islands emerging from solid-state dewetting. We hope that our work will motivate further experimental investigations to control the size and spatial order of nanoscale islands via solid-state dewetting of stressed solid films.

*Corresponding author.

francesco.boccardo@univ-lyon1.fr

†Corresponding author.

olivier.pierre-louis@univ-lyon1.fr

- [1] P. de Gennes, F. Brochard-Wyart, and D. Quere, *Capillarity and Wetting Phenomena: Drops, Bubbles, Pearls, Waves* (Springer, New York, 2003).
- [2] R. V. Craster and O. K. Matar, *Rev. Mod. Phys.* **81**, 1131 (2009).
- [3] D. Bonn, J. Eggers, J. Indekeu, J. Meunier, and E. Rolley, *Rev. Mod. Phys.* **81**, 739 (2009).
- [4] J. H. Snoeijer and B. Andreotti, *Annu. Rev. Fluid Mech.* **45**, 269 (2013).
- [5] C. V. Thompson, *Annu. Rev. Mater. Res.* **42**, 399 (2012).
- [6] *Trends and Perspectives in Solid-State Wetting/Mouillage Solide-Solide: Tendances et Perspectives*, edited by O. Pierre-Louis (Springer, New York, 2013), Vol. 14.
- [7] F. Leroy, L. Borowik, F. Cheynis, Y. Almadori, S. Curiotto, M. Trautmann, J. Barb, and P. Müller, *Surf. Sci. Rep.* **71**, 391 (2016).
- [8] O. Pierre-Louis, *Prog. Cryst. Growth Charact. Mater.* **62**, 177 (2016).
- [9] R. Nuryadi, Y. Ishikawa, and M. Tabe, *Appl. Surf. Sci.* **159–160**, 121 (2000).
- [10] B. Yang, P. Zhang, D. E. Savage, M. G. Lagally, G.-H. Lu, M. Huang, and F. Liu, *Phys. Rev. B* **72**, 235413 (2005).
- [11] D. T. Danielson, D. K. Sparacin, J. Michel, and L. C. Kimerling, *J. Appl. Phys.* **100**, 083507 (2006).
- [12] E. Dornel, J.-C. Barbé, F. de Crécy, G. Lacolle, and J. Eymery, *Phys. Rev. B* **73**, 115427 (2006).
- [13] E. Bussmann, F. Cheynis, F. Leroy, P. Müller, and O. Pierre-Louis, *New J. Phys.* **13**, 043017 (2011).
- [14] F. Leroy, F. Cheynis, T. Passanante, and P. Müller, *Phys. Rev. B* **85**, 195414 (2012).
- [15] F. Cheynis, F. Leroy, T. Passanante, and P. Müller, *Appl. Phys. Lett.* **102**, 161603 (2013).
- [16] Z. A. Burhanudin, R. Nuryadi, Y. Ishikawa, and M. Tabe, *Thin Solid Films* **508**, 235 (2006).
- [17] G. Capellini, G. Ciasca, M. De Seta, A. Notargiacomo, F. Evangelisti, and M. Nardone, *J. Appl. Phys.* **105**, 093525 (2009).
- [18] M. Naffouti, R. Backofen, M. Salvalaglio, T. Bottein, M. Lodari, A. Voigt, T. David, A. Benkouider, I. Fraj, L. Favre, A. Ronda, I. Berbezier, D. Grosso, M. Abbarchi, and M. Bollani, *Sci. Adv.* **3** (2017).
- [19] J. Ye and C. V. Thompson, *Appl. Phys. Lett.* **97**, 071904 (2010).
- [20] J. Ye and C. V. Thompson, *Phys. Rev. B* **82**, 193408 (2010).
- [21] J. Ye and C. V. Thompson, *Acta Mater.* **59**, 582 (2011).
- [22] G. H. Kim, R. V. Zucker, J. Ye, W. C. Carter, and C. V. Thompson, *J. Appl. Phys.* **113**, 043512 (2013).
- [23] E. Jiran and C. V. Thompson, *J. Electron. Mater.* **19**, 1153 (1990).
- [24] E. Jiran and C. V. Thompson, *Thin Solid Films* **208**, 23 (1992).
- [25] C. Kenefick and R. Raj, *Acta Metal.* **37**, 2947 (1989).
- [26] A. Kosinova, O. Kovalenko, L. Klinger, and E. Rabkin, *Acta Mater.* **83**, 91 (2015).
- [27] J. Ye and C. V. Thompson, *Adv. Mater.* **23**, 1567 (2011).
- [28] H. Wong, P. Voorhees, M. Miksis, and S. Davis, *Acta Mater.* **48**, 1719 (2000).
- [29] A. Pimpinelli and J. Villain, *Physics of Crystal Growth* (Cambridge University Press, Cambridge, England, 1998).
- [30] V. A. Shchukin and D. Bimberg, *Rev. Mod. Phys.* **71**, 1125 (1999).
- [31] J.-N. Aqua, I. Berbezier, L. Favre, T. Frisch, and A. Ronda, *Phys. Rep.* **522**, 59 (2013).
- [32] F. Rovaris, R. Bergamaschini, and F. Montalenti, *Phys. Rev. B* **94**, 205304 (2016).
- [33] R. J. Asaro and W. A. Tiller, *Metall. Mater. Trans. B* **3**, 1789 (1972).
- [34] M. A. Grinfeld, *J. Nonlinear Sci.* **3**, 35 (1993).
- [35] W. T. Tekalign and B. J. Spencer, *J. Appl. Phys.* **96**, 5505 (2004).
- [36] M. S. Levine, A. A. Golovin, S. H. Davis, and P. W. Voorhees, *Phys. Rev. B* **75**, 205312 (2007).
- [37] J.-N. Aqua, T. Frisch, and A. Verga, *Phys. Rev. B* **76**, 165319 (2007).
- [38] R. Bergamaschini, M. Salvalaglio, R. Backofen, A. Voigt, and F. Montalenti, *Adv. Phys.* **1**, 331 (2016).
- [39] A. K. Tripathi and O. Pierre-Louis, *Phys. Rev. E* **97** (2018).
- [40] A. K. Tripathi and O. Pierre-Louis, *Phys. Rev. E* **101**, 042802 (2020).
- [41] L. Borowik, N. Chevalier, D. Mariolle, F. Bertin, A. Chabli, and J.-C. Barb, *J. Appl. Phys.* **114**, 063502 (2013).
- [42] F. Cheynis, E. Bussmann, F. Leroy, T. Passanante, P. Mü, and N. Iler, *Int. J. Nanotechnology* **9**, 396 (2012).
- [43] W. W. Mullins, *J. Appl. Phys.* **28**, 333 (1957).
- [44] B. J. Spencer, P. W. Voorhees, and S. H. Davis, *J. Appl. Phys.* **73**, 4955 (1993).
- [45] See Supplemental Material, which includes Refs. [46–54], at <http://link.aps.org/supplemental/10.1103/PhysRevLett.128.026101> for details on surface diffusion equation, normalized dynamical model, wetting potential, numerical methods, dependence of $\bar{\lambda}_0$ and $\bar{\tau}_0$ on θ_{eq} , equilibrium island

- shapes, decrease of L_0 due to wetting effects, calculation of λ_∞ for sSOI, comparison between the linearized and the full elastic model, dewetting dynamics of a square, film with n equal to 3, 4 and 5.
- [46] J. Israelachvili, *Intermolecular and Surface Forces* (Elsevier Science, New York, 2015).
- [47] S. Cox and P. Matthews, *J. Comput. Phys.* **176**, 430 (2002).
- [48] M. Frigo and S. Johnson, *Proc. IEEE* **93**, 216 (2005).
- [49] A. Logg, K.-A. Mardal, G.N. Wells *et al.*, *Automated Solution of Differential Equations by the Finite Element Method* (Springer, New York, 2012).
- [50] G. Schifani, T. Frisch, M. Argentina, and J.-N. Aqua, *Phys. Rev. E* **94**, 042808 (2016).
- [51] A. Constantinescu, L. Golubović, and A. Levandovsky, *Phys. Rev. E* **88**, 032113 (2013).
- [52] A. K. Swarnakar, O. V. der Biest, and J. Vanhellefont, *Phys. Status Solidi C* **11**, 150 (2014).
- [53] M. T. Kim, *Thin Solid Films* **283**, 12 (1996).
- [54] D. Srolovitz and S. Davis, *Acta Mater.* **49**, 1005 (2001).
- [55] C.-h. Chiu, *Appl. Phys. Lett.* **75**, 3473 (1999).
- [56] M. Ortiz, E. Repetto, and H. Si, *J. Mech. Phys. Solids* **47**, 697 (1999).
- [57] W. T. Tekalign and B. J. Spencer, *J. Appl. Phys* **96**, 5505 (2004).
- [58] M. Khenner, *Phys. Rev. B* **77**, 165414 (2008).
- [59] N. Tretyakov, M. Miller, D. Todorova, and U. Thiele, *J. Chem. Phys.* **138**, 064905 (2013).
- [60] J. Eggers, *Phys. Rev. Lett.* **80**, 2634 (1998).
- [61] J. Ye and C. V. Thompson, *Appl. Phys. Lett.* **97**, 071904 (2010).
- [62] T. Barsotti, J. Bermond, and M. Drechsler, *Surf. Sci.* **146**, 467 (1984).
- [63] P. Lazar and M. Otyepka, *Phys. Rev. B* **91**, 115402 (2015).
- [64] D. Matsunaka and Y. Shibutani, *Phys. Rev. B* **77**, 165435 (2008).
- [65] J. Chen and N. Chen, *J. Phys. Condens. Matter* **22**, 215001 (2010).
- [66] J. Blakely and H. Mykura, *Acta Metall.* **9**, 23 (1961).
- [67] P. Nozières, *J. Phys. I France* **3**, 681 (1993).
- [68] W. H. Yang and D. J. Srolovitz, *Phys. Rev. Lett.* **71**, 1593 (1993).
- [69] K. Kassner and C. Misbah, *Phys. Rev. E* **66**, 026102 (2002).
- [70] O. Pierre-Louis and Y. Saito, *Eur. Phys. Lett.* **86**, 46004 (2009).
- [71] M. Dufay and O. Pierre-Louis, *Phys. Rev. Lett.* **106**, 105506 (2011).
- [72] A. Chame, Y. Saito, and O. Pierre-Louis, *Phys. Rev. Mater.* **4**, 094006 (2020).
- [73] O. E. Shklyaev, M. J. Miksis, and P. Voorhees, *J. Mech. Phys. Solids* **54**, 2111 (2006).
- [74] B. J. Spencer and J. Tersoff, *Phys. Rev. Lett.* **79**, 4858 (1997).
- [75] M. S. McCallum, P. W. Voorhees, M. J. Miksis, S. H. Davis, and H. Wong, *J. Appl. Phys.* **79**, 7604 (1996).
- [76] M. Salvalaglio, P. Zaumseil, Y. Yamamoto, O. Skibitzki, R. Bergamaschini, T. Schroeder, A. Voigt, and G. Capellini, *Appl. Phys. Lett.* **112**, 022101 (2018).
- [77] D. T. Danielson, D. K. Sparacin, J. Michel, and L. C. Kimerling, *J. Appl. Phys.* **100**, 083507 (2006).
- [78] W. Kan and H. Wong, *J. Appl. Phys.* **97**, 043515 (2005).
- [79] R. V. Zucker, G. H. Kim, W. C. Carter, and C. V. Thompson, *C. R. Phys.* **14**, 564 (2013), trends and perspectives in solid-state wetting/Mouillage solide-solide: Tendances et perspectives.
- [80] T. Watanabe, H. Fujiwara, H. Noguchi, T. Hoshino, and I. Ohdomari, *Japanese J. Appl. Phys.* **38**, L366 (1999).
- [81] G.-H. Lu and F. Liu, *Phys. Rev. Lett.* **94**, 176103 (2005).
- [82] M. J. Beck, A. van de Walle, and M. Asta, *Phys. Rev. B* **70**, 205337 (2004).
- [83] A. H. Carim, *J. Electrochem. Soc.* **134**, 741 (1987).
- [84] A. Auberton-Hervé, T. Barge, F. Metral, M. Bruel, B. Aspar, C. Maleville, H. Moriceau, and T. Poumeyrol, *MRS Proc.* **446**, 177 (1996).
- [85] T. Yoshinobu, A. Iwamoto, K. Sudoh, and H. Iwasaki, *J. Vac. Sci. Technol. B* **13**, 1630 (1995).
- [86] E.-C. Cho, M. A. Green, J. Xia, R. Corkish, and A. Nikulin, *J. Appl. Phys.* **96**, 3211 (2004).
- [87] L. Tsetseris and S. T. Pantelides, *Phys. Rev. Lett.* **97**, 116101 (2006).
- [88] S. Bhattacharjee, C.-H. Ko, and M. Elimelech, *Langmuir* **14**, 3365 (1998).
- [89] E. M. Hoek and G. K. Agarwal, *J. Colloid Interface Sci.* **298**, 50 (2006).
- [90] J. Becker, G. Grün, R. Seemann, H. Mantz, K. Jacobs, K. R. Mecke, and R. Blossey, *Nat. Mater.* **2**, 59 (2003).
- [91] R. Fetzer, M. Rauscher, R. Seemann, K. Jacobs, and K. Mecke, *Phys. Rev. Lett.* **99**, 114503 (2007).
- [92] J. A. Diez, A. G. González, and R. Fernández, *Phys. Rev. E* **93**, 013120 (2016).
- [93] Q. Zhao, W. Jiang, and W. Bao, *SIAM J. Sci. Comput.* **42**, B327 (2020).
- [94] T. Vilmin and E. Raphaël, *Eur. Phys. J. E* **21**, 161 (2006).
- [95] P. Damman, S. Gabriele, S. Coppée, S. Desprez, D. Villers, T. Vilmin, E. Raphaël, M. Hamieh, S. A. Akhrass, and G. Reiter, *Phys. Rev. Lett.* **99**, 036101 (2007).